# Estimating Surface Oil Extent from the Deepwater Horizon Oil Spill using ASCAT Backscatter

Richard D. Lindsley and David G. Long

Microwave Earth Remote Sensing Laboratory
Brigham Young University
Provo, UT 84602

*Abstract*—**The damping effects of oil on capillary ocean waves alter the backscattered power of radar measurements made by remote-sensing instruments such as scatterometers. Numerically computed vector winds are input to a wind geophysical model function (GMF) to determine the expected backscatter from the ocean surface uncontaminated by surface oil. Large differences between expected backscatter and observed backscatter indicate areas of the ocean surface affected by oil. The recent oil spill from the *Deepwater Horizon* rig in the Gulf of Mexico provides a spatial extent large enough to be tracked by the ASCAT scatterometer. In this paper we use ASCAT data and numerically predicted winds to estimate the spatial extent of surface oil.**

## I. INTRODUCTION

The oil spill from the *Deepwater Horizon* oil rig in the Gulf of Mexico is one of the largest environmental disasters in recent history. The consequences from the roughly 4.4 million barrels [1] leaked will continue long after the 15 July 2010 capping of the well. A time-series estimate of the extent and shape of the oil on the ocean surface is beneficial for estimating the amount of oil as a function of time and its effects on ocean life and human industries.

Active microwave sensors are often preferred for remote detection of oil spills by virtue of their all-weather performance in both day and night conditions. Historically, SAR (Synthetic Aperture Radar) instruments have been used since the spatial resolution—on the order of a hundred meters or less for a spaceborne SAR—is fine enough to resolve many oil spills [2]. Scatterometers are a related class of active microwave instruments with a resolution that is more coarse—on the order of a few kilometers. The processes that enable oil detection using SAR images are the same for scatterometer data.

Remarkably, the spatial extent of the Deepwater Horizon oil slick is large enough to be resolvable by ASCAT (Advanced Scatterometer), particularly when processed with resolution-enhancement algorithms. By exploiting the effects of surface oil on ocean waves, a coarse estimate of surface extent is made by examining data processed from ASCAT.

ASCAT is a spaceborne wind scatterometer that operates on the MetOp-A platform. Like other wind scatterometers, ASCAT indirectly measures near-surface vector ocean winds at a height of 10 meters ($U_{10}$) by directly measuring backscattered power over the ocean at various azimuth angles. An empirically derived geophysical model function (GMF) relates backscatter with $U_{10}$ vector winds.

This paper examines a method of estimating surface oil extent by comparing ASCAT-measured backscatter with the expected backscatter using the GMF and numerical weather predicted (NWP) winds. Background information on ASCAT, the GMF, and the effects of surface oil are first presented. Our methodology for surface oil extent mapping follows. Results are shown for selected case studies and the performance of the presented method is evaluated.

## II. BACKGROUND

Launched in 2006 aboard MetOp-A, ASCAT is in a sun-synchronous polar orbit. It is a real-aperture scatterometer operating in the C-band (5.255 GHz) with three fan beams on either side of the MetOp ground track. This forms approximately a 1460-km-wide ground swath with a 360-km-wide gap at nadir. ASCAT operates in vertical-polarization mode only [3].

The normalized radar cross-section, $\sigma^0$, is measured by each of the six antennas. The CMOD5.n GMF relates $\sigma^0$ as a function of $U_{10}$ and other parameters, including the incidence angle and the azimuth angle relative to wind direction [4].

Using an estimate of the ASCAT spatial $\sigma^0$ measurement response on the Earth for each measurement and making use of overlapping measurements, high-resolution reconstruction of the surface $\sigma^0$ can be formed [5], [6]. This high-resolution $\sigma^0$ image is the basis of UHR ASCAT wind, a wind product containing ultra-high resolution (UHR) $U_{10}$ vector wind.

At the oblique incidence angle range used for scatterometers, the mechanism for radar backscatter due to ocean surface roughness is attributed, to first order, to Bragg scattering. When ocean wave wavelengths of $\lambda_o$ fulfill the Bragg resonance condition

$$\lambda_o = n\lambda_r/2\sin\theta_i, \quad n = 1, 2, \ldots, \qquad (1)$$

where $\lambda_r$ is the radar wavelength and $\theta_i$ is the incidence angle, the electromagnetic waves constructively self-interfere to enhance the surface $\sigma^0$ value [7]. For the radar frequency and range of incidence angles used by ASCAT, ocean waves with a range of 3.5–6.7 cm are responsible for Bragg scattering ($n = 1$).

While the Bragg waves are typically modulated by longer waves, Bragg waves are generally in equilibrium with near-surface wind speed. Higher winds generate more Bragg waves,

leading to greater $\sigma^0$ values for higher winds. Because oil has higher viscosity than that of sea water, oil on the ocean surface dampens the amplitude of Bragg waves. This modifies the $\sigma^0$ of the affected area because the smoother ocean surface reflects less microwave power back to the scatterometer. The $\sigma^0$ measurement of the oil-contaminated area is thus lower than the oil-free case [2], [8], [9].

While surface oil dominates Bragg wave dampening, other sources can also decrease the backscatter. These include biogenic oil slicks produced by plankton and fish, natural oil seeps from the ocean floor, organic wastes from fish processing ships, and changes in the water-ocean interface, such as that from upwelling [8]. Though covering a much smaller area than the Deepwater Horizon spill, these sources can lead to false positives in oil spill detection, often referred to as "look-alikes." Techniques to reduce look-alikes include multi-frequency and multi-polarization instruments, using *a priori* knowledge of geographic information, historical human and animal activity, and shipping lanes, and using different remote sensors that detect oil under mechanisms different than Bragg scattering (such as microwave radiometers or infrared, optical, or ultraviolet sensors) [2], [8]. Since this paper only considers a single-frequency, single-polarization microwave instrument, we expect some false positives in addition to detected surface oil.

Another challenge to oil detection is that it is wind speed-dependent. If winds are too low ($< 3$ m/s), the ocean surface is not sufficiently roughened to provide a contrast between the oil-contaminated surface and the oil-free surface. Additionally, if the winds are too high ($> 7$-$10$ m/s), the surface oil mixes down into the water and may be less detectable. Previous papers have recognized the importance of factoring wind speed in to surface oil detection [2], [9], and have done so, for example, as part of synergistic data methods [10]. Rather than relying solely upon $\sigma^0$ measurements to detect oil, the method presented in this paper incorporates the effects of wind as part of the detection process.

## III. METHOD

We detect surface oil by comparing the expected backscatter with the actual backscatter. An expected $\sigma^0$ value may be determined by computing the GMF based on local wind conditions. Truth winds may come from various sources, but NWP winds are used here for two reasons. First, NWP winds are reported as uniform spatial samples. This simplifies collocation with ASCAT data as opposed to using spatially isolated measurements, such as from ships or buoys. Secondly, the CMOD5.n GMF is tuned for NWP winds. Using NWP winds with CMOD5.n applies the close relationship between NWP winds and C-band radar backscatter [4].

The difference between the expected $\sigma^0$ (from NWP data) and the measured $\sigma^0$ (from ASCAT) is

$$\sigma^0_{\text{NWP}} - \sigma^0_{\text{ASCAT}} = \epsilon, \tag{2}$$

where $\epsilon$ is an error term. While some error is anticipated from noise, the expected value of $\epsilon$ is positive in the presence of oil

due to the damping effects of the oil on the surface spectrum. Large values of $\epsilon$ may be used to detect and map the surface oil extent.

For the analysis, both ECMWF-computed (European Centre for Medium-range Weather Forecasts) and NCEP-computed (National Centers for Environmental Prediction) $U_{10}$ are used as numerical winds. Since the results are very similar between the two, only ECMWF winds results are shown below.

Unfortunately the temporal and spatial sampling of NWP winds and ASCAT UHR winds differ fairly significantly. These differences are explained in the next section. However, the NWP winds are treated as ground truth for the purposes of this study. On account of the loose definition of "truth winds" in this case, our oil extent estimates are somewhat coarse. Even so, as shown below, there is good correlation between our ASCAT-detected oil estimates and other sources, including satellite-derived surface oil analyses from the National Oceanic and Atmospheric Administration (NOAA).

### A. Expected backscatter

The NWP data has a coarser spatial and temporal resolution than for ASCAT. NWP winds are computed every six hours every $1°$ in latitude and longitude. We bilinearly interpolate the two vector wind fields nearest in time to an ASCAT pass over the oil spill. For each ASCAT $\sigma^0$ measurement ($\sigma^0_{\text{ASCAT}}$), the two bilinearly interpolated wind fields are then interpolated in time, forming a trilinear interpolation to find the NWP wind data corresponding to each value of $\sigma^0_{\text{ASCAT}}$. The collocated and interpolated NWP wind data is passed through the CMOD5.n GMF to find the $\sigma^0$ value corresponding to the given wind vector, $\sigma^0_{\text{NWP}}$.

While this permits a pointwise comparison of $\sigma^0_{\text{ASCAT}}$ with $\sigma^0_{\text{NWP}}$, linear interpolation low-pass filters the data. The interpolated $\sigma^0_{\text{NWP}}$ therefore has limited high-frequency spatial content. With this caveat in mind, a direct comparison of $\sigma^0_{\text{ASCAT}}$ with $\sigma^0_{\text{NWP}}$ subtracts the low-frequency expected backscatter from $\sigma^0_{\text{ASCAT}}$ but preserves any small-scale structure.

### B. Measured backscatter

While a polar-orbiting instrument makes many daily observations of the poles, low-latitude coverage is more sparse. The Deepwater Horizon oil spill is located around $29°$ latitude, just outside the tropics. A maximum of two passes per day is possible (ascending and descending), but in practice only about eight passes per 10-day period cover the spill region.

For each location in the ASCAT swath, generally three $\sigma^0$ measurements exist, one each for the antenna "looks": fore, mid, and aft. The middle look is at a slightly different range of incidence angles than the fore and aft looks. High resolution $\sigma^0$ reconstruction is performed for each look using the AVE algorithm. The AVE algorithm is a weighted average of each $\sigma^0$ measurement on a high-resolution grid using estimates of the ground footprint of each measurement [5], [11].

### C. Backscatter error

Using NWP wind data, the $\sigma^0_{\text{ASCAT}}$ measurement geometry (including incidence and azimuth angles), and the GMF, the
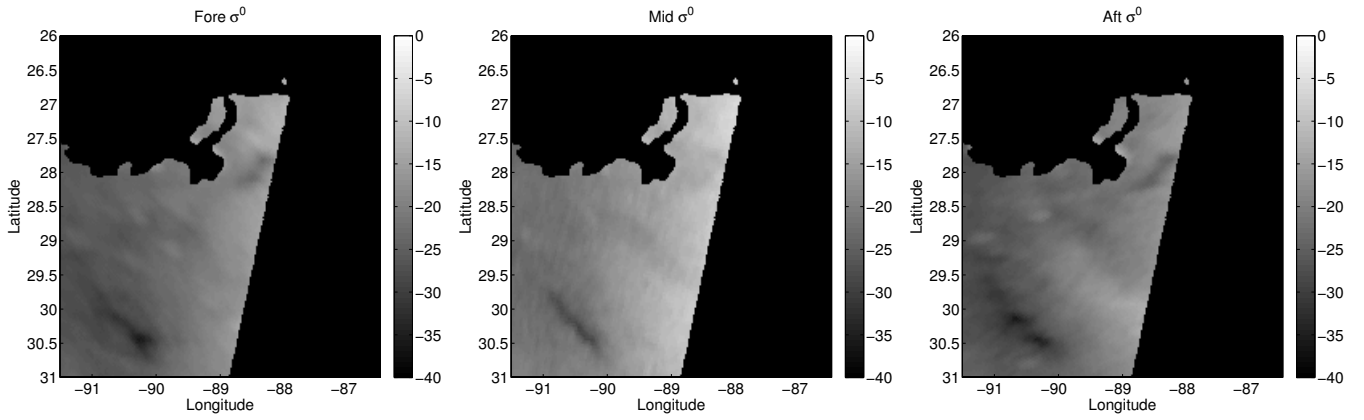
Fig. 1. ASCAT $\sigma^0$ fore, middle, and aft looks for rev 19221 (3 July 2010). Fore and aft looks span incidence angles of 36–55° and the middle look spans a range of 27–44°.
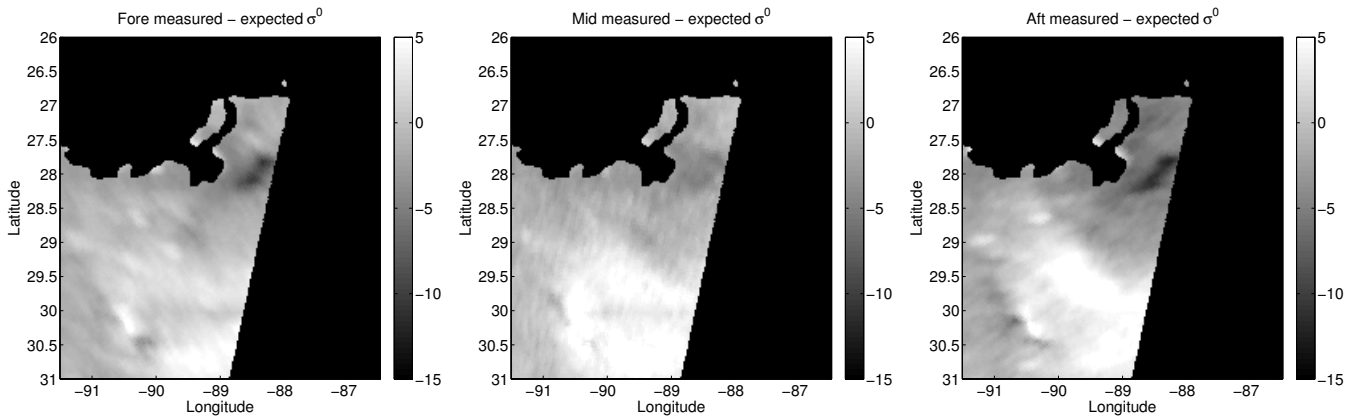


Fig. 2. Difference between $\sigma^0_{\text{ASCAT}}$ and $\sigma^0_{\text{NWP}}$ for ASCAT rev 19221 (3 July 2010). Compare with Fig. 1.

corresponding $\sigma^0_{\text{NWP}}$ is computed for each $\sigma^0_{\text{ASCAT}}$ look. To define a single metric for oil surface extent, the three looks are combined as follows. Using (2) for each look, we stack the three $\epsilon$ errors into a vector $\vec{\epsilon} = [\epsilon_{\text{fore}} \ \epsilon_{\text{mid}} \ \epsilon_{\text{aft}}]^T$. The $\ell_2$ norm, defined as

$$\| \vec{\epsilon} \|_2 = \sqrt{\epsilon_{\text{fore}}^2 + \epsilon_{\text{mid}}^2 + \epsilon_{\text{aft}}^2}, \qquad (3)$$

is used as a metric to map the surface oil extent by combining data from all available looks.

### D. Oil extent validation

In order to validate the results, products from the Experimental Marine Pollution Surveillance Report (EMPSR) are used. The EMPSR is an experimental product produced by NOAA that utilizes SAR and visible imagery from satellites to estimate the surface oil extent of the spill [12]. It is assumed for this paper that the EMPSR product is an accurate representation of the true oil extent, owing to the previous good results using SAR and visible imagery to detect surface oil.

The EMPSR product used is the daily composite shapefile, a vector-based geospatial representation of surface oil extent based on the available satellite imagery for the day. Not every day has an available EMPSR product, so only ASCAT passes that coincide with EMPSR data are used.

### IV. RESULTS

For the duration of the oil leak, 204 ASCAT passes over the spill region are available. Out of these, 118 have corresponding EMPSR data, and 11 are selected as case studies. As outlined above, for each ASCAT pass, the measured $\sigma^0$ for each look is compared with the $\sigma^0_{\text{NWP}}$ obtained from NWP winds and the CMOD5.n GMF. To illustrate the advantage of using NWP winds, we compare the results using both the methodology described above and a method that does not account for winds.

Figure 1 shows the high-resolution $\sigma^0$ field over each of the three looks for an ascending pass of ASCAT. In these images, two potential oil regions can be seen: one east of the Mississippi River Delta and one further south of the delta. Similarly, Fig. 2 shows the difference between $\sigma^0_{\text{ASCAT}}$ and $\sigma^0_{\text{NWP}}$ for each of the three looks. In this case, the region south of the delta with low wind speeds is accounted for, leaving only the oil region east of the delta.

Combining the three looks of Fig. 1 by taking the $\ell_2$ norm of the $\sigma^0$ images, similar to Eqn. (3), results in Fig. 3a. The middle look (center image of Fig. 1) spans a lower incidence
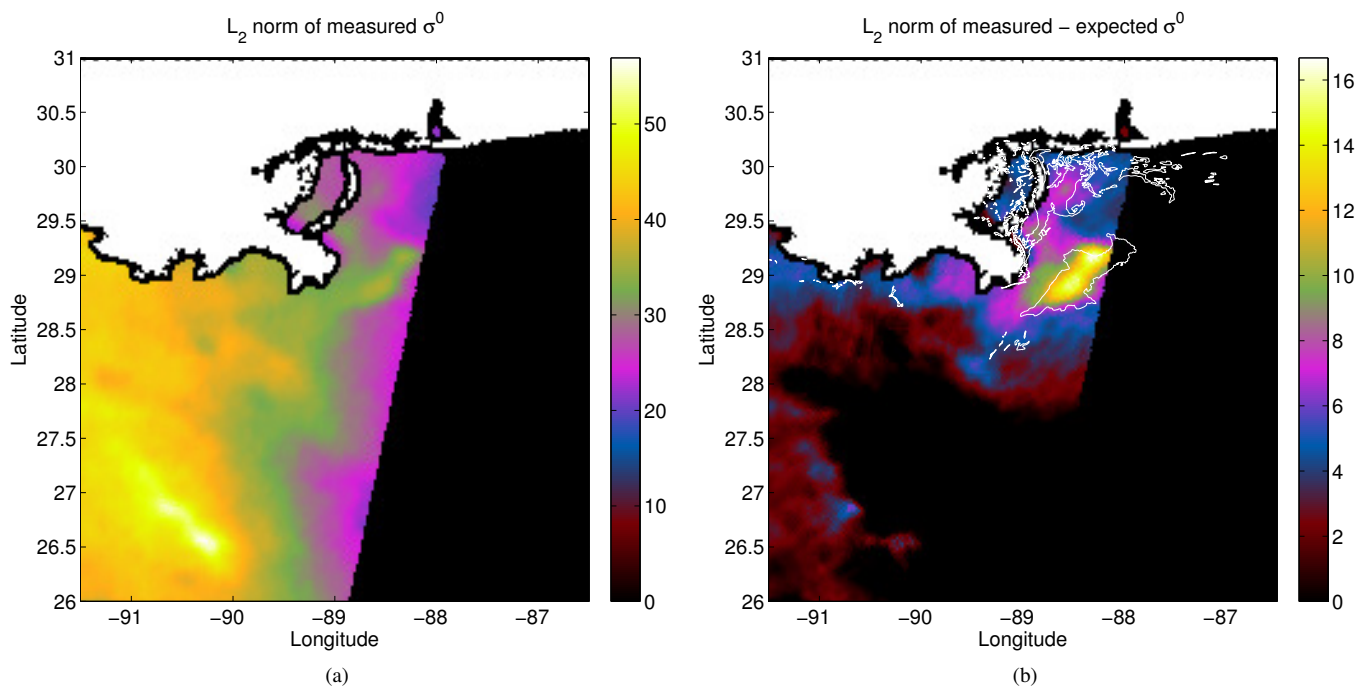
Fig. 3. The $\ell_2$ norm of the measured $\sigma^0$ in (a), and the $\ell_2$ norm of the difference between measured and expected $\sigma^0$ in (b). Data from ASCAT rev 19221 (3 July 2010) is used, along with interpolated ECMWF winds for (b). Land is masked out and near-coastal regions are set to 0 to remove biased wind estimates. The bright area in (b) indicates suppresed $\sigma^0$ measurements due to the presence of surface oil. The white outline is the EMPSR analysis for the surface oil extent.
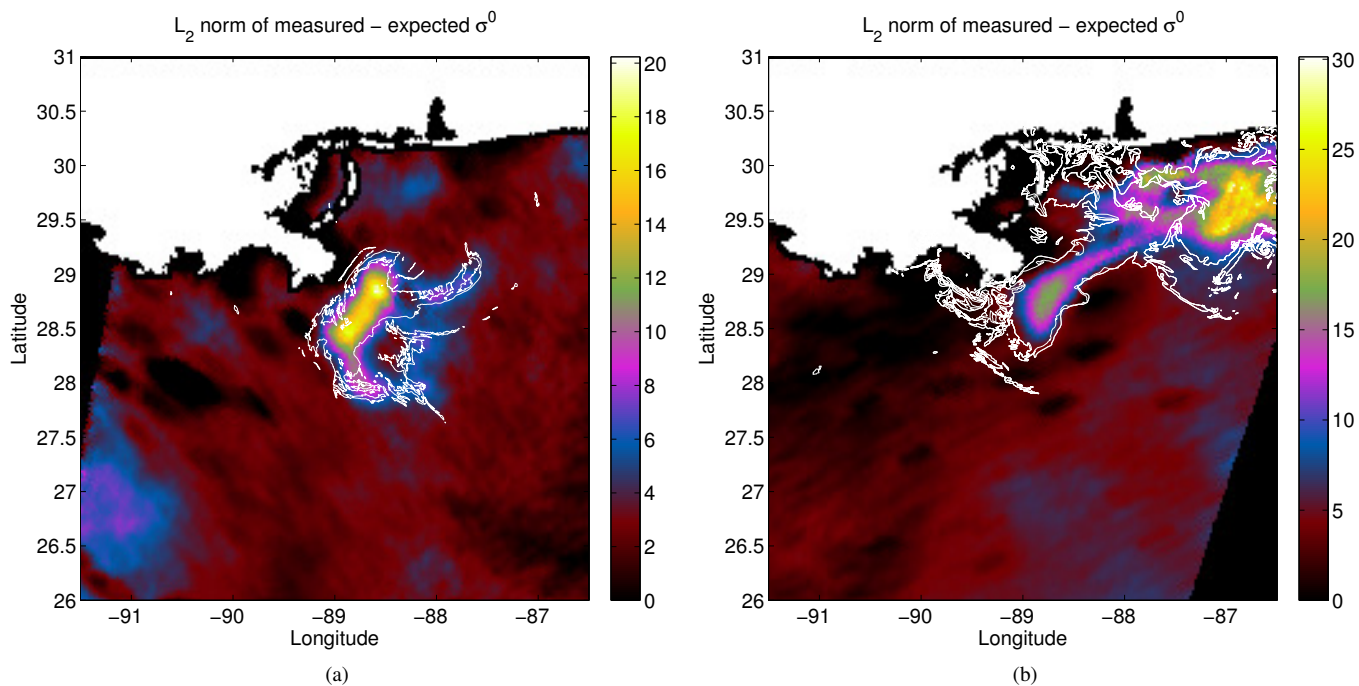


Fig. 4. Same as Fig. 3b, but (a) is for ASCAT rev 19434 (18 July 2010), and (b) is for ASCAT rev 19122 (26 June 2010).

angle range than the other two, leading to poor detection of the first oil candidate region. The $\ell_2$ norm of the three looks has a greater value for the second candidate region than the first. The second region is a false positive due to low wind speeds in the area.

Using Eqn. (3) to merge the three looks of Fig. 2 results in Fig. 3b. The white outline is the EMPSR product for the day. In this case, the results agree well with the largest EMPSR oil region, while the smaller regions near the coast are not as well defined.

Two more ASCAT passes are shown in Fig. 4a and Fig. 4b. These passes again show a good match with EMPSR results. In general, the EMPSR results corroborate with the method presented here during the middle of the spill (late April – mid July), and are less effective near the beginning or end of the spill. At these times, the density of surface oil does not appreciably dampen $\sigma^0$.

## V. CONCLUSION

The detection of ocean surface oil by active microwave instruments is based on a contrast of $\sigma^0$ over oil-affected areas and oil-free areas. Moderate wind speeds sufficiently roughen the ocean surface to provide this contrast. A comparison of $\sigma^0$ values while accounting for the wind over the oil improves the detection.

The method presented in this paper accounts for the near-surface wind by using the ASCAT GMF in conjunction with NWP winds to compute an expected backscatter, $\sigma^0_{\mathrm{NWP}}$. The difference between the expected backscatter due to the winds and the actual backscatter measured by ASCAT is then evaluated for oil detection, as expressed in Eqn. (2).

The results presented show a good match with conventional oil detection techniques making use of multiple sensors as processed in the EMPSR product. False positives, or oil "look-alikes" still arise owing to the limitations of working with a single instrument, but the occurrence of wind-related false alarms is diminished. Results validate well with EMPSR results except for the very beginning and end of the spill. It is possible that this method could be used in conjunction with more sophisticated detection and classification algorithms.

## REFERENCES

[1] T. J. Crone and M. Tolstoy, "Magnitude of the 2010 gulf of mexico oil leak," *Science*, vol. 330, no. 6004, p. 634, 2010. [Online]. Available: http://www.sciencemag.org/content/330/6004/634.abstract

[2] C. Brekke and A. Solberg, "Oil spill detection by satellite remote sensing," *Remote Sensing of Environment*, vol. 95, no. 1, pp. 1–13, 2005.

[3] J. Figa-Saldaña, J. J. W. Wilson, E. Attema, R. Gelsthorpe, M. R. Drinkwater, and A. Stoffelen, "The advanced scatterometer (ASCAT) on the meteorological operational (MetOp) platform: A follow on for European wind scatterometers," *Canadian Journal of Remote Sensing*, vol. 28, no. 3, pp. 404–412, 2002.

[4] H. Hersbach, "Cmod5.n: A c-band geophysical model function for equivalent neutral wind," ECMWF, Tech. Rep., 2008. [Online]. Available: http://www.ecmwf.int/publications/library/ecpublications/_pdf/tm/501-600/tm554.pdf

[5] R. D. Lindsley and D. G. Long, "Adapting the SIR algorithm to ASCAT," in *Proc. IEEE Int. Geoscience and Remote Sensing Symp. (IGARSS)*, 2010, pp. 3402–3405.

[6] D. S. Early and D. G. Long, "Image reconstruction and enhanced resolution imaging from irregular samples," *IEEE Trans. Geosci. Remote Sens.*, vol. 39, no. 2, pp. 291–302, 2001.

[7] F. Ulaby, R. Moore, and A. Fung, *Microwave Remote Sensing: Active and Passive*, D. Simonett, Ed.  Artech House, Inc, 1986, vol. 2.

[8] P. Clemente-Colón and X. Yan, "Low-backscatter ocean features in synthetic aperture radar imagery," *Johns Hopkins APL Technical Digest*, vol. 21, no. 1, pp. 116–121, 2000.

[9] W. Alpers, "Remote Sensing of Oil Spills," in *Maritime Disaster Management Symposium*, 2002, pp. 19–23.

[10] F. Girard-Ardhuin, G. Mercier, F. Collard, and R. Garello, "Operational oil-slick characterization by SAR imagery and synergistic data," *IEEE J. Ocean. Eng.*, vol. 30, no. 3, p. 487, 2005.

[11] D. G. Long, P. Hardin, and P. Whiting, "Resolution enhancement of spaceborne scatterometer data," *IEEE Trans. Geosci. Remote Sens.*, vol. 31, no. 3, pp. 700–715, 1993.

[12] Satellite Derived Surface Oil Analysis Products - Deepwater Horizon. NOAA/NESDIS. [Online]. Available: http://www.ssd.noaa.gov/PS/MPS/deepwater.html